Organic Geochemistry 124 (2018) 215–227

Contents lists available at ScienceDirect

Organic Geochemistry

journal homepage: www.elsevier.com/locate/orggeochem

Depositional environment of the Late Santonian lacustrine source rocks in the Songliao Basin (NE China): Implications from organic geochemical analyses

Xiaoning Tong [a,c], Jianfang Hu [a,*], Dangpeng Xi [b], Mengbo Zhu [a,c], Jianzhong Song [a], Ping'an Peng [a]

[a] State Key Laboratory of Organic Geochemistry, Guangzhou Institute of Geochemistry, Chinese Academy of Sciences, Guangzhou 510640, China
[b] State Key Laboratory of Biogeology and Environmental Geology, China University of Geosciences, Beijing 100083, China
[c] University of Chinese Academy of Sciences, Beijing 100049, China

ARTICLE INFO

Article history:
Received 13 February 2018
Received in revised form 30 July 2018
Accepted 30 July 2018
Available online 1 August 2018

Keywords:
Santonian
Organic-rich sediments
Biomarkers
Water column stratification
Seawater incursion events

ABSTRACT

The Songliao Basin (SLB) located in northeastern China is one of the largest Cretaceous continental sedimentary basins in the world. The SLB is filled with sediments deposited in the Upper Jurassic, the Lower Cretaceous and the Upper Cretaceous epochs. The Nenjiang Formation (K_2n) is subdivided into five members, where Member 2 (K_2n^2) was deposited in the late Santonian in the lower part of the Nenjiang Formation. This member is characterized by a thick succession of organic-rich source rocks. However, the complexity of the depositional environment raises questions about the specific factors that drove this accumulation of organic material. Here, we present data on the total organic carbon (TOC) contents and their stable carbon isotope values ($\delta^{13}C_{org}$), as well as biomarker data from 50 outcrop samples collected from the Yuewangcheng (YWC) section, in the southeastern SLB. According to the variations of the bulk organic parameters (TOC and $\delta^{13}C_{org}$) and biomarker indices, the profile could be divided into three stages (stages I–III). The distribution of biomarkers (*n*-alkanes, steranes and hopanes) and $\delta^{13}C_{org}$ values indicate that the organic matter (OM) in the Lower K_2n^2 is derived largely from algae and macrophytes, with a minor input from bacteria and land plants. The water column was stratified, as indicated by the presence of gammacerane. Variations in the pristane/phytane (Pr/Ph) and aryl isoprenoids relative to phenanthrene ratio (A-i/P) suggest that bottom waters were anoxic during Stage I (31.5–26.0 m) and Stage II (26.0–16.3 m), with the anoxic layer impinging on the euphotic zone and a relative oxic environment at Stage III (16.3–0 m). This brackish environment persisted in the water over the interval represented by the section, as reflected by methytrimethyltridecyl chromans (MTTCs) Index (MTTCI) and α-MTTC/γ-MTTC ratios. Marine transgressions, with subsequent seawater incursions, can be detected with the presence of 24-*n*-propyl-cholestanes and 24-isopropyl-cholestanes in the Lower K_2n^2 sediments, especially during Stage I. These seawater incursions are closely correlated with anoxic conditions and the deposition of organic-rich source rocks.

1. Introduction

The Cretaceous was an interval of greenhouse climate (Bice et al., 2006), with high sea levels and intermittent oceanic anoxia (Schlanger and Jenkyns, 1976; Haq et al., 1987; Skelton et al., 2003; Jenkyns, 2010; Hu et al., 2012; Haq, 2014). Most of our knowledge of the greenhouse climate and anoxic events in Earth's history comes from marine sedimentary records. In contrast, there are few studies of Cretaceous continental deposits (Wang et al., 2013). The Songliao Basin (SLB), which contains a complete succession of Cretaceous terrestrial sediments (Feng et al., 2010), is an ideal place to study the evolution of Late Cretaceous terrestrial biotas, paleoenvironments, and paleoclimates.

Based on the palynological data, Gao et al. (1999) argued that although the Cretaceous atmospheric temperature changed frequently in the SLB, the SLB had a subtropical environment. The most significant data related to reconstructing Cretaceous climate in the SLB are gathered from ostracod oxygen isotope measurements from the SK-1 borehole covering the Turonian to Maastrichtian interval (Chamberlain et al., 2013). These ostracod records present a distinct negative shift in isotope values during the Turonian, followed by an increasing trend from the late

* Corresponding author at: Guangzhou Institute of Geochemistry, Chinese Academy of Sciences, Guangzhou, GD 510640, China.
E-mail address: hujf@gig.ac.cn (J. Hu).

https://doi.org/10.1016/j.orggeochem.2018.07.018
0146-6380/

Turonian through the early Campanian (Chamberlain et al., 2013). These trends from the terrestrial SLB are similar to those seen in global marine records (Friedrich et al., 2012), although the magnitude of the isotopic shift is much larger in the SLB. This difference may be due to amplification effects, such as changes in the temperature or relative humidity at the sites of evaporation over the ocean, or changes in temperature in the regional drainage network (Chamberlain et al., 2013; Wang et al., 2013).

The massive, organic-rich source rocks (i.e., dark mudstones, oil shales, and black shales) in the SLB are concentrated in the lower part of the Nenjiang Formation (K_2n^{1+2}). Paleoenvironmental conditions during deposition of the oil shales in K_2n^{1+2} have attracted considerable attention (Wang et al., 2011; Bechtel et al., 2012; Jia et al., 2013). Bechtel et al. (2012) proposed that the source rocks were deposited in a deep, aerobic, and eutrophic freshwater lacustrine environment. Jia et al. (2013) suggested that high biological productivity was the major controlling factor leading to organic matter (OM) enrichment in the SLB.

Recent lines of evidence, including the discovery of foraminifera (Xi et al., 2016), detection of 24-*n*-propyl-cholestanes and 24-isopropyl-cholestanes (Hu et al., 2015; Cao et al., 2016a), and negative excursions of $\delta^{34}S$ (Cao et al., 2016b), suggest that multiple marine transgressions occurred during the deposition of the lower K_2n^2, and the subsequent deposition of hydrocarbon source rocks may be related to these transgressions.

The conditions leading to the deposition of organic-rich source rocks in the SLB are still debated, with evolution of the lacustrine environment and changes in the global carbon cycle being two possible explanations. A detailed investigation into environment changes during the Late Santonian is crucial for understanding the relationship between changing environmental conditions and oil shale formation in lacustrine settings.

In this study, we generated a high-resolution record of bulk OM and biomarker data from an outcrop located in the southeastern SLB, with the goal of reconstructing paleoenvironmental conditions in a lacustrine environment during the Late Santonian. We assessed the degree of water column stratification, redox conditions, and water salinity, and discuss the role of marine incursion events, in order to better understand the relationship between paleoenvironment conditions and the deposition of organic-rich source rocks in the SLB.

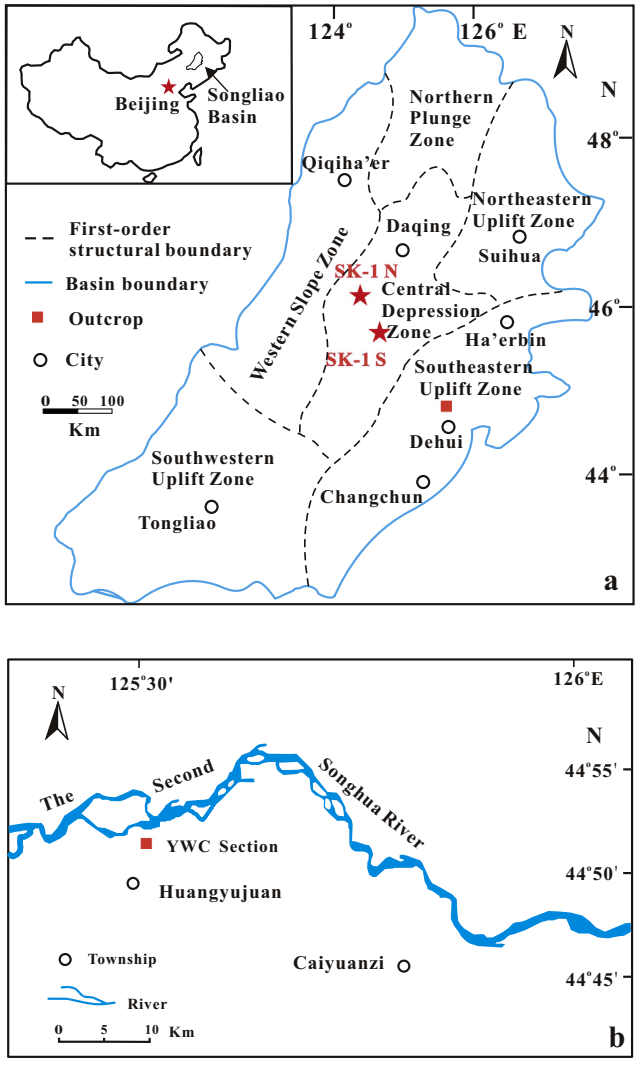

Fig. 1. Sketch map showing the locality of study area: (a) Location of Songliao Basin showing the six first-order tectonic units, cores SK-1 (N and S) and Yuewangcheng (YWC) section; (b) The location of YWC section.

2. Geologic setting and sampling program

The Songliao Basin, located in northeastern China, is the largest Cretaceous continental rift basin in the world (Fig. 1a). The modern SLB is approximately 750 km in length and 350 km in width, with an area of 260 000 km^2. The tectonic evolution of the basin was influenced by two Late Mesozoic active continental margins: the Mongol-Okhotsk Belt to the north and northwest and Sikhote-Alin Orogenic Belt to the east (Wang et al., 2016a). Two regional angular unconformities separate the basin fill into three tectonostratigraphic sequences. The first is a syn-rift volcanogenic succession, which was deposited from 150 to 105 Ma. This was followed by a post-rift sedimentary succession from 105 to 79.1 Ma, then a structural inversion sequence from 79.1 to 64 Ma (Wang et al., 2016a). Based on features of the basin fill exposed at the surface, the SLB can be divided into six first-order structural units: the western slope zone, the northern plunge zone, the central depression zone, the northeastern uplift zone, the southeastern uplift zone, and the southwestern uplift zone (Fig. 1a).

With a complete Cretaceous succession of organic-rich continental sediments, the SLB is one of China's most valuable oil and gas producing regions. The Nenjiang Formation (K_2n) is one such unit, deposited during the post-rift thermal subsidence stage. Early in the deposition of K_2n^2, the entire basin, with an area of 200 000 km^2, was occupied by deep-water lacustrine facies (Feng et al., 2010).

For this study, 50 samples were collected from the Yuewangcheng (YWC) section (44°52′17″N, 125°30′17.41″E), located on the southern bank of the Second Songhua River, in the southeastern part of the SLB (Fig. 1b). The YWC section is 32.3 m in total stratigraphic thickness, and consists of mudstones, black shales and oil shales (Fig. 2b). As these lithologies are widespread in the SLB, the YWC section can be lithostratigraphically correlated with the SK-1 borehole (Fig. 2a). The K_2n^1/K_2n^2 boundary is characterized by a distinct marker bed of black shale interbedded with oil shale, allowing the YWC section to be assigned to the upper K_2n^1 and lower K_2n^2. The age of the K_2n is late Santonian to middle Campanian (84.5–79.1 Ma) which has been constrained by high-resolution SIM/TIMS zircon U-Pb ages (He et al., 2012; Wang et al., 2016b), magnetostratigraphy (Deng et al., 2013), and astronomical tuning from the SK–1 Core (Wu et al., 2013; 2014). A zircon U-Pb age of 83.5 ± 0.5 Ma was also obtained from the base of the YWC section, at 30.76 m (Yu, 2017). Wan et al. (2017) demonstrated that the Cretaceous Normal Superchron ended at 83.07 ± 0.15 Ma, with this date also serving as an estimate for the age of the Santonian–Campanian stage boundary. Based on lithostratigra-

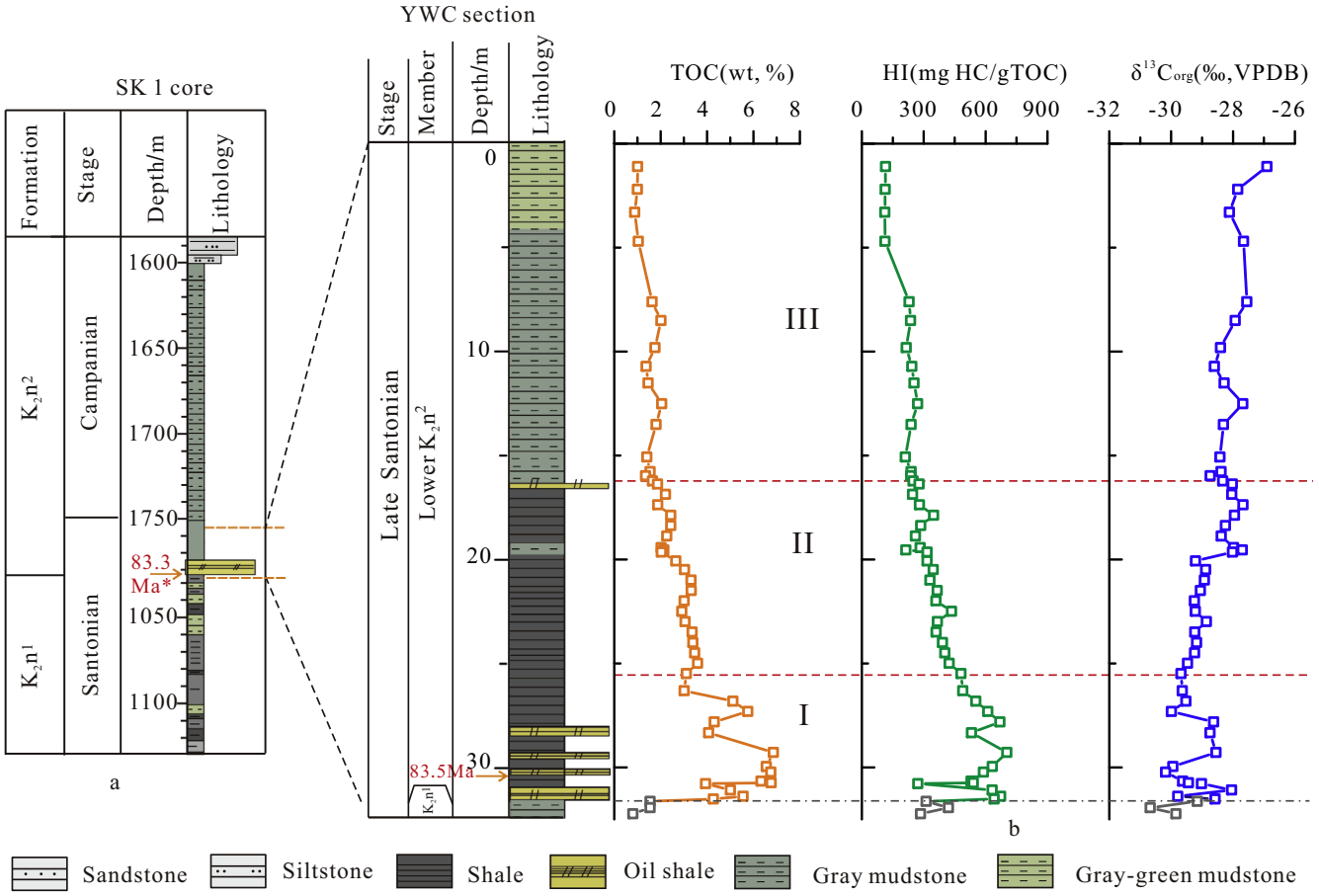

Fig. 2. (a) Correlation of Late Santonian Stratigraphy between SK-1 cores (N and S) (Wang et al., 2013) and YWC section. The TIMS U-Pb zircon radiometric age (Wang et al., 2016b) is marked by a red character. The marker bed of black shale interbedded with oil shale was identified in the bottom of the YWC section, suggesting that the YWC section could be related to the lower Member 2 of Nenjiang Formation (K_2n^2); (b) Depth variation of bulk geochemical parameters, including total organic carbon (TOC), hydrogen index (HI) and isotopic composition of organic carbon ($\delta^{13}C_{org}$) in lower K_2n^2 from the YWC section. (For interpretation of the references to colour in this figure legend, the reader is referred to the web version of this article.)

phy and sediment thickness, it was concluded that the top of the YWC section does not reach the Santonian–Campanian stage boundary, with the entire YWC section restricted to the late Santonian (Fig. 2b).

3. Analytical methods

3.1. Bulk organic analysis

The samples were first cleaned with distilled water, dried at 50 °C and crushed to a fine powder. Subsamples (150 mg) were prepared for analysis of organic carbon (OC) content and the isotopic composition of organic carbon ($\delta^{13}C_{org}$), by treating them with 4 N HCl to remove carbonate, then rinsing with distilled water and freeze-drying. The OC content and $\delta^{13}C_{org}$ of the carbonate-free samples were then measured on a Pyro Cube Elemental Analyzer coupled to an Isoprime 100 continuous flow isotope ratio mass spectrometer (IRMS). Detailed methods and instrumental conditions for OC analysis are described in Xie et al. (2016). Carbon isotope results are reported in ‰, relative to the Vienna Peedee Belemnite (VPDB) standard. The analytical precision was better than 3% (RSD) for OC content, and 0.3‰ for $\delta^{13}C_{org}$. Each sample was analyzed in duplicate, with the mean of the two measurements reported in this study. Pyrolysis analyses were carried out using a Vinci Rock-Eval VI instrument following the standard procedure after Espitalié et al. (1977) and Lafargue et al. (1998). The parameters measured by this analysis included the TOC (wt%), S1 (mg HC/g rock), S2 (mg HC/g rock), S3 (mg CO_2/g rock) and T_{max} (the temperature at which the S2 peak is highest, °C). Values for the Hydrogen Index (HI) and Oxygen Index (OI) were calculated as S2 × 100/TOC and S3 × 100/TOC, respectively.

3.2. Biomarker analysis

A representative aliquot of each sample was extracted for organic geochemical analysis using a Soxhlet apparatus, with a 9:1 (v/v) dichloromethane (DCM)/methanol (MeOH) solution. After 72 h of extraction, the solvent was allowed to evaporate, and the residues were dissolved in hexane to remove asphaltenes. The soluble fraction was separated into aliphatic, aromatic, and polar fractions via alumina/silica gel column chromatography, using hexane, hexane/DCM (2:1, v/v), and DCM/MeOH (1:1, v/v), respectively.

The saturated hydrocarbon fraction was analyzed using an Agilent 7890B gas chromatograph (GC) with a J&W HP-1MS fused silica column (60 m × 0.25 mm i.d.; 0.25 μm film thickness), coupled to a flame ionization detector (FID) to obtain data on *n*-alkanes, pristane and phytane. The injector and detector temperatures were 290 °C and 300 °C, respectively. Samples were injected in splitless mode with N_2 carrier gas. The oven temperature was initially 80 °C (held for 2 min), followed by a programmed increase to 150 °C at a rate of 15 °C/min, then to a maximum temperature of 300 °C (held for 30 min) at a rate of 5 °C/min.

The saturated and aromatic fractions were analyzed using a Thermo TRACE gas chromatograph equipped with a 60 m J&W DB-5MS fused silica column (0.32 mm i.d.; 0.25 μm film thickness), coupled to a Thermo DSQII quadrupole mass spectrometer (MS) with an electron impact ion source at 70 eV. The initial oven temperature was 80 °C (held for 2 min), with a programmed increase to 120 °C at a rate of 15 °C/min, followed by a more gradual increase at 4 °C/min to a maximum temperature of 300 °C (held for 30 min). Samples were injected in splitless mode with helium carrier gas, at a flow rate of 1.5 mL/min. The injector and ion source temperatures were 290 °C and 230 °C, respectively; the MS scan range was *m/z* 50 to 650. Fragment ions of *m/z* 191, 217, 133 were chosen for identification of hopanoids, steranes, and aryl isoprenoids, respectively. Fragment ions of *m/z* 121, 135, 149 were chosen for identification of methytrimethyltridecyl chromans (MTTCs).

C_{30} sterane biomarkers were analyzed using a ThermoFinnigan TSQ Quantum XLS UltraTriple Quadrupole GC–MS-MS with a DB-5MS fused silica capillary column (50 m × 0.32 mm i.d.; 0.25 μm film thickness). The injector and ion source temperatures were 300 °C and 250 °C, respectively. The instrument was run in MRM mode, with an initial temperature of 110 °C (held for 2 min) followed by a programmed increase to 240 °C at a rate of 10 °C/min, and a further increase to 305 °C (held for 20 min) at a rate of 2 °C/min. A deuterated C_{27} sterane standard (d4-ααα (20R)-cholestane) was added (50–250 ng) as an internal standard to quantify the sterane biomarker content. Yields assume equal mass spectral response factors between analytes. Compound quantification was performed by peak area integration of *m/z* 98 and 217 in the extracted ion chromatogram for dinosteranes and 24-propyl-cholestanes, respectively. Analytical errors were estimated to be lower than 5% for target compounds. Detailed methods are described in Hu et al. (2015).

4. Results

4.1. Bulk organic matter

The total organic carbon (TOC) and HI values range from 0.80 to 6.86 wt% and from 112 to 703 mg HC/g TOC respectively (Table 1, Fig. 2b). Variations in HI and TOC are correlated throughout the section (Fig. 2b). The YWC section consists of the uppermost K_2n^1 and the lower K_2n^2 (Fig. 2b). The uppermost K_2n^1 is characterized by low TOC and HI values which is significantly different from those for the lower K_2n^2 member. This paper is focused on the paleoenvironmental changes of the lower K_2n^2 member since this contains the thickest organic source rock in the YWC section

Based on the stratigraphic variation in TOC and the HI, the late Santonian lower K_2n^2 succession can be divided into three stages (Table 1, Fig. 2b). Stage I (31.5–26.0 m) is characterized by the highest TOC values (3.01–6.86%) and negative $\delta^{13}C_{org}$ values (−30.2‰ to −28.0‰). Stage II covers the interval from 26.0 to 16.3 m and exhibits a decreasing trend in TOC (1.87–3.59%) coupled with less negative $\delta^{13}C_{org}$ values. Stage III, from 16.3 to 0 m, has relatively low TOC content (0.88–2.05%), with $\delta^{13}C_{org}$ values with an interval from −28.7‰ to −26.9‰, more positive than those seen in stages I and II. In general, the $\delta^{13}C_{org}$ profile varies inversely with the TOC profile (Fig. 2b). The HI vs OI diagram shows that the OM presents types I and II kerogen in Stage I. Most of the OM is types II and III kerogen in stages II and III (Fig. 3). The HI values show a considerable variation for the lower K_2n^2, and the range of values are generally higher than 500 mg HC/gTOC in Stage I and relatively lower in the range 112–248 mg HC/gTOC in Stage III. The T_{max} values for OM in our samples range from 430 °C to 441 °C (Table 1).

Table 1
Values for TOC, HI, T_{max}, 20S/(20R + 20S) ratios of C_{29} sterane, ββ/(αα+ββ) of C_{29} steranes and 22S/(22S + 22R) ratio of C_{31} hopanes in samples from the YWC section.

Stage	Depth (m)	TOC (wt%)	HI (mg HC/gTOC)	T_{max} (°C)	C_{29}20S/(20R + 20S)	C_{29}ββ/(αα+ββ)	C_{31}22S/(22S + 22R)
III	1.10	1.01	115	439	0.05	0.24	0.11
	2.20	1.00	113	438	0.03	0.23	0.11
	3.30	0.88	112	439	0.05	0.24	0.11
	4.70	1.04	112	436	0.03	0.23	0.11
	7.60	1.63	229	440	0.03	0.24	0.11
	8.51	2.01	236	435	0.04	0.25	0.10
	9.81	1.76	216	435	0.04	0.22	0.10
	10.71	1.38	243	440	0.04	0.23	0.08
	11.51	1.46	253	439	0.05	0.25	0.10
	12.51	2.05	270	437	0.03	0.22	0.08
	13.51	1.80	239	438	0.03	0.22	0.07
	15.07	1.41	211	437	0.04	0.22	0.12
	15.77	1.54	239	436	0.03	0.20	0.14
	15.97	1.35	237	441	0.03	0.21	0.12
	16.22	1.65	248	438	0.02	0.19	0.11
II	16.37	1.87	278	436	0.02	0.18	0.20
	16.87	2.21	246	435	0.03	0.20	0.13
	17.37	1.88	280	436	0.03	0.21	0.13
	17.87	2.44	348	436	0.02	0.23	0.07
	18.37	2.44	286	437	0.04	0.20	0.10
	18.87	2.26	260	434	0.03	0.19	0.06
	19.43	2.02	283	437	0.02	0.20	0.16
	19.54	2.14	214	434	0.02	0.19	0.12
	19.64	2.03	316	435	0.02	0.20	0.09
	20.07	2.66	317	435	0.04	0.21	0.09
	20.49	3.03	347	431	0.04	0.20	0.10
	20.99	3.31	331	435	0.05	0.22	0.06
	21.49	3.32	365	431	0.03	0.23	0.00
	21.99	3.02	359	436	0.02	0.19	0.12
	22.49	2.92	435	434	0.04	0.20	0.14
	22.99	3.06	367	435	0.03	0.20	0.16
	23.49	3.36	360	432	0.04	0.19	0.16
	23.99	3.39	391	435	0.03	0.19	0.08
	24.49	3.47	403	434	0.03	0.19	0.18
	24.99	3.59	424	436	0.04	0.21	0.11
	25.49	3.11	481	436	0.04	0.19	0.19
I	26.31	3.01	490	433	0.03	0.17	0.14
	26.81	5.11	552	435	0.03	0.17	0.09
	27.31	5.76	611	435	0.03	0.17	0.11
	27.81	4.31	669	436	0.04	0.17	0.11
	28.33	4.07	532	430	0.04	0.16	0.14
	29.28	6.86	703	433	0.03	0.15	0.14
	29.96	6.55	632	431	0.05	0.16	0.12
	30.23	6.75	590	436	0.04	0.14	0.16
	30.66	6.33	530	434	0.04	0.16	0.24
	30.74	6.77	541	430	0.04	0.19	0.13
	31.09	5.00	632	436	0.06	0.22	0.15
	31.39	5.55	673	440	0.04	0.15	0.15
	31.52	4.27	642	440	0.05	0.17	0.16

4.2. Biomarkers

4.2.1. n-Alkanes and the Pr/Ph ratio

n-Alkanes from *n*-C_{11} to *n*-C_{31} were detected (Fig. 4a). The relative proportions of *n*-alkanes of the C_{15-20}, C_{21-25} and C_{27-31} ranges were 22.3–58.1%, 33.8–61.6%, and 5.4–31.8%, respectively (Table 2). The CPI_{27-31} (carbon preference index, Bray and Evans, 1961) values range from 4.3 to 9.2, indicating that the *n*-alkanes exhibit obvious odd predominance (Table 2). Pr/Ph ratios range from 0.35 to 1.21, with the lowest values in Stage I (Fig. 5).

4.2.2. Steranes

Steranes were detected in all samples, including regular steranes, 4α-methylsteranes, and C_{30} steranes (Fig. 4b). The 5β,14α,17α(H) isomers are present in the C_{27}–C_{29} range. The carbon number distribution of regular steranes is $C_{29} > C_{27} > C_{28}$ for

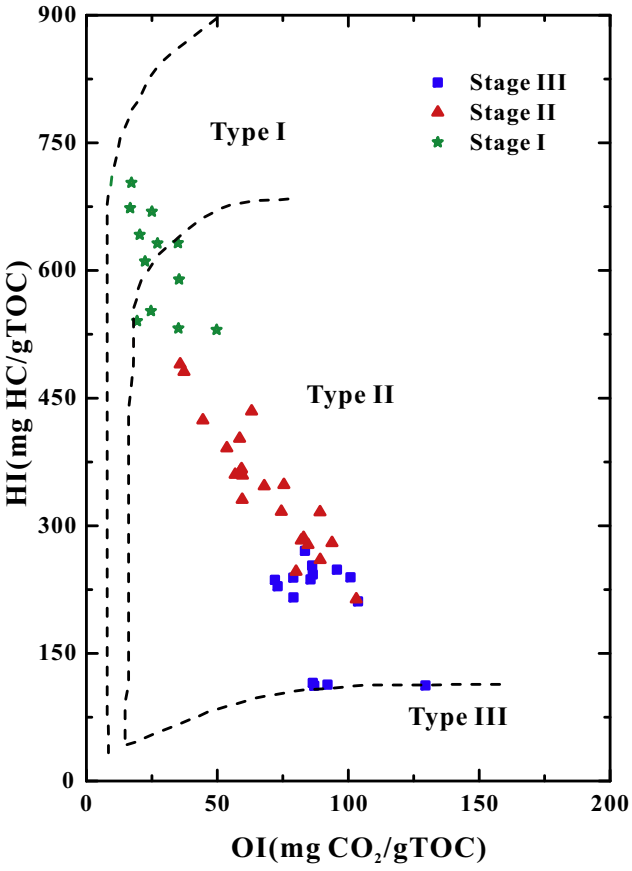

Fig. 3. Cross-plot of HI vs oxygen index (OI) showing the organic matter types for Yuewangcheng section samples. Dashed lines for the three kerogen types are also shown.

all samples (Fig. 4b); the C_{27}/C_{29} ratio varies from 0.35 to 0.72 (Table 2). C_{28}–C_{30} 4α-methylsteranes were also detected. A number of different C_{30} steranes, including dinosteranes (4,23,24-trimethylcholestanes), 24-*n*-propyl-cholestanes, and 24-isopropyl-cholestanes were detected (Fig. 4f), in concentrations in the range 0.06–4.57 μg/g, 1.53–59.4 μg/g, and 1.1–60.3 μg/g, respectively (Fig. 6). Highest concentrations of C_{30} steranes were present in Stage I.

4.2.3. Hopanoids and gammacerane

The distribution of hopanoids is characterised by the presence of 17α,21β(H)- and 17β,21α(H)-hopanes ranging from C_{27} to C_{32}, with C_{28} hopanes absence; the most abundant hopanoid was 17α,21β-22R C_{30} hopane (Fig. 4d). Gammacerane was also detected in samples from the YWC section (Fig. 4d), and the Gammacerane Index (gammacerane/C_{30} αβ-hopane) ranged from 0.05 to 0.29 (Fig. 5).

4.2.4. Methytrimethyltridecyl chromans

Methytrimethyltridecyl chromans (MTTCs) are present throughout the entire section (Fig. 4e); these include trimethylated 2-methyl-2-(4,8,12-trimethyltridecyl) chromans (α-MTTC), dimethylated 2-methyl-2-(4,8,12-trimethyltridecyl) chromans (β-MTTC, γ-MTTC and ζ-MTTC) and monomethylated 2-methyl-2-(4,8,12- trimethyltridecyl) chromans (δ-MTTC) (Sinninghe Damsté et al., 1989). The MTTC Index (MTTCI) is defined as a ratio of α-MTTC relative to the total MTTCs. Values of the MTTCI varied between 0.54 and 0.74 (Fig. 5). The α-MTTC/γ-MTTC (α/γ) ratio ranged from 2.30 to 6.82, displaying similar trends with MTTCI (Fig. 5).

4.2.5. Aryl isoprenoids

C_{14}–C_{22} aryl isoprenoids (A-i) were found only in stage I and II samples (Fig. 4c). These compounds are present only in low abundance, with C_{14} aryl isoprenoids being the most common. The ratio of aryl isoprenoids to phenanthrene (A-i/P ratio) ranged from 0.15 to 1.2 (Fig. 5).

5. Discussion

5.1. Maturity assessment

Low T_{max} values (430–441 °C) indicate that the OM is immature to low maturity in the lower Member 2 of the Nenjiang Formation (Table 1). The 22S/(22S + 22R) ratios of the 17α,21β(H)-C_{31} hopanes were between 0.06 and 0.24 (with a mean of 0.12) in the samples of the lower K_2n^2. These values are distinctly lower than the end point value of ca. 0.6 and are in agreement with the T_{max} values. Moreover, the 20S/(20R + 20S) ratios of C_{29} steranes range from 0.02 to 0.06 suggest low maturity of the OM. Therefore, this variation in the biomarker indices is not related to differences in the maturity.

5.2. Sources of organic matter in the YWC section

As shown in Fig. 3, the OM is Type I and II kerogen in Stage I, suggesting that the OM is mainly derived from lake algae and aquatic macrophytes. While the OM is Type II kerogen in stages II and III, which indicates that the contribution of the lake phytoplankton to the OM declined. Therefore, the sources of OM in the YWC section are predominantly from algae and aquatic macrophytes. The distribution of *n*-alkanes may also reflect the origin of OM. Short-chain alkanes ($<C_{20}$) are predominantly found in algae (Cranwell, 1977), while medium-chain alkanes (C_{21}–C_{25}) are mainly derived from aquatic macrophytes (Ficken et al., 2000), and long-chain alkanes ($>C_{27}$) with a predominance of odd carbon-numbers are sourced from land plants (Eglinton and Hamilton, 1967). The alkanes are characterized by relatively high proportions of C_{15-20} and C_{21-25} alkanes (15.4–58.1% and 33.8–61.6% respectively) and lower proportion of C_{27-31} alkanes (5.4–40.1%) (Fig. 4a; Table 2). This composition suggests that the OM is mostly derived from algae and aquatic macrophytes, with a small contribution from land plants. The high CPI values also suggest that the OM derived from minor land plant contributions (Tissot et al., 1974). However, a possible origin of long chain *n*-alkanes from microalgae has to be taken into account (Volkman et al., 1998). For instance, *Botryococcus braunii* (race A) is known to biosynthesise exclusively odd carbon numbered *n*-alkadienes and trienes in the C_{25}–C_{31} carbon number range and may contribute to the C_{27}–C_{31} *n*-alkanes (Metzger et al., 1991). The *n*-alkane composition is characterized by a relatively higher proportion of long-chain alkanes in stages I and III than in Stage II, suggesting an increased contribution from land plants and/or *B. braunii* (race A) to the OM in stages I and III.

The distribution of regular steranes also has the potential to record the sources of OM. In the past, organic geochemists have attributed C_{27} steranes to algae, whereas C_{29} steranes to land plants (Volkman, 1986). However, some data suggest the C_{29} sterols can also originate from green algae in old rocks (Kodner et al., 2008). The regular steranes exhibit $C_{29} > C_{27}$ in the lower K_2n^2 member. The molecular composition of *n*-alkanes suggests that land plant input to the SLB OM pool is lower than that of the algae and macrophytes. Therefore, green algae might contribute some

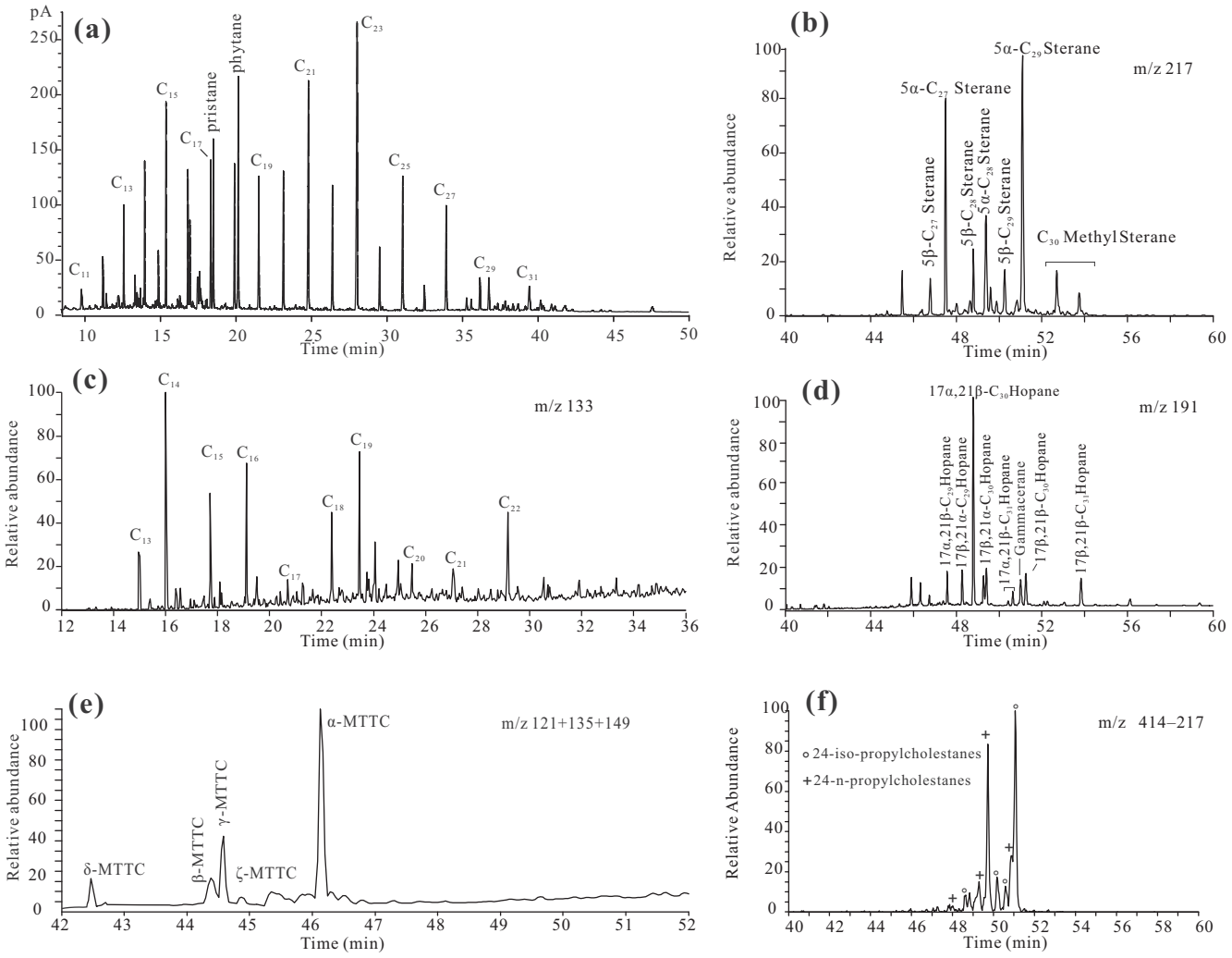

Fig. 4. (a) Representative gas chromatograms of the aliphatic hydrocarbon fractions showing the distribution of *n*-alkanes, pristane (Pr) and phytane (Ph) in the lower K_2n^2 from the YWC section; (b) Representative mass chromatograms of *m/z* 217 showing the identification of steranes in the lower K_2n^2; (c) Representative mass chromatograms of *m/z* 133 showing the identification of aryl isoprenoids in lower K_2n^2; (d) Representative mass chromatograms of *m/z* 191 showing the identification of hopanes in the lower K_2n^2; (e) Partial mass chromatograms (*m/z* 121 + 135 + 149) for methyltrimethyltridecyl chromans (MTTCs) in the lower K_2n^2; (f) Representative MRM chromatograms showing the identification of 24-*n*-propylcholestanes and 24-isopropylcholestanes in the lower K_2n^2.

portion of C_{29} steranes in the SLB. The similar carbon isotopic values of C_{27} and C_{29} steranes from the Nenjiang Formation in the SLB also support this hypothesis (Wang et al., 2015). The relatively high concentration of 4-methyl steranes might be derived from dinoflagellates. Hou et al. (2000) has confirmed the presence of fossil dinoflagellates in the Upper Cretaceous oil shales and found that dinosteranes were the predominant C_{30} methyl steranes in the SLB.

A series of C_{30} steranes has been identified as definitive biomarkers of marine organic input in sedimentary rocks and petroleum, allowing marine sediments and hydrocarbons to be distinguished from their non-marine counterparts (Moldowan, 1984). These diagnostic steranes include 24-*n*-propyl-cholestanes and 24-isopropyl-cholestanes, which are produced exclusively by marine pelagophyte algae (Moldowan et al., 1990) and marine demosponges (Love et al., 2009) respectively. These compounds were detected in all samples from the lower K_2n^2 (Fig. 6), indicating marine OM input. The highest abundance of C_{30} steranes occurred in Stage I, and may reflect a relatively large contribution of marine algae in this interval.

Hopanes are found in the lipid cell membranes of many bacterial groups, including cyanobacteria, heterotrophic bacteria, methanotrophs and chemoautotrophs (Sinninghe Damsté and Koopmans, 1997). The detection of hopanes in samples from the YWC section indicates bacterial OM input. The ratio of steranes/hopanes (Ste/Hop) can potentially reflect the relative contributions of algae and bacteria. According to Mackenzie et al. (1984), low values are characteristic of lacustrine environments, or facies influenced by specific bacterial groups, while high values indicate marine, algal-dominated OM. In the present study, the high Ste/Hop ratios in Stage I probably reflect eutrophication and high biological productivity in the photic zone, with only a limited contribution from bacteria (Peters et al., 2005). The relatively low Ste/Hop values (Table 2) in stages II and III are likely to indicate stronger bacterial degradation and relatively poor OM preservation, which is in agreement with the relatively high Pr/Ph ratios (Fig. 2).

Gammacerane is derived from tetrahymanol, a biomarker originating in bacteriovorus ciliates that typically live at or below the chemocline (Sinninghe Damsté et al., 1995). The detection of gammacerane in all samples from the YWC section indicates that at least some of the sedimentary OM derives from secondary consumers (Fig. 4d), and that the water column was likely stratified. Specific aryl isoprenoids, which are interpreted as derived from photosynthetic green sulfur bacteria (Summons and Powell, 1987), were detected in stages I and II, implying that these bacteria

Table 2
Biomarker ratios in samples from the YWC section.

	Depth	*n*-alkanes (%)			CPI_{27-31}	Ste/Hop	C_{27}/C_{29} Sterane
	(m)	$\sum n\text{-}C_{15-20}$	$\sum n\text{-}C_{21-25}$	$\sum n\text{-}C_{27-31}$			
III	1.1	44.1	35.0	20.8	5.6	1.8	0.65
	2.2	46.1	40.8	13.2	5.8	2.1	0.52
	3.3	40.5	40.6	18.9	5.6	2.3	0.52
	4.7	51.2	36.9	11.8	6.5	1.9	0.45
	7.6	40.4	45.7	13.9	6.0	1.4	0.51
	8.51	47.0	45.2	7.8	6.0	1.7	0.67
	9.81	42.4	47.9	9.8	7.1	2.4	0.50
	10.71	43.0	44.8	12.1	6.6	2.4	0.49
	11.51	40.6	48.3	11.1	5.9	3.1	0.54
	12.51	47.9	40.0	12.1	5.8	1.5	0.56
	13.51	51.5	38.9	9.6	5.4	1.4	0.47
	15.07	49.3	40.5	10.2	4.9	3.8	0.49
	15.77	38.1	46.8	15.1	6.0	4.8	0.42
	15.97	35.9	48.7	15.4	5.5	5.7	0.44
	16.22	40.2	46.0	13.9	6.3	3.0	0.41
II	16.37	28.7	54.0	17.3	7.0	2.5	0.39
	16.87	45.1	46.6	8.3	5.3	1.5	0.42
	17.37	45.4	46.7	7.9	6.0	1.6	0.47
	17.87	37.2	53.4	9.4	6.2	2.0	0.55
	18.37	30.4	61.6	8.0	7.6	1.3	0.49
	18.87	45.9	48.2	5.9	8.5	1.5	0.37
	19.43	52.4	37.1	10.5	5.8	1.6	0.31
	19.54	58.1	33.8	8.1	6.1	1.6	0.28
	19.64	55.2	38.1	6.7	6.1	1.8	0.42
	20.07	43.4	51.2	5.4	6.2	1.5	0.44
	20.49	37.3	54.5	8.3	6.6	1.5	0.51
	20.99	35.9	54.2	9.9	6.8	1.1	0.46
	21.49	35.3	55.0	9.8	6.6	1.1	0.5
	21.99	41.8	51.0	7.2	5.8	1.8	0.49
	22.49	40.9	50.0	9.2	6.0	1.5	0.46
	22.99	34.9	56.7	8.4	6.5	1.3	0.42
	23.49	40.3	53.2	6.5	6.9	1.3	0.45
	23.99	43.0	50.9	6.1	5.1	1.3	0.47
	24.49	39.8	50.1	10.1	6.4	1.3	0.48
	24.99	47.6	43.9	8.5	5.4	3.5	0.62
	25.49	51.0	40.8	8.2	5.4	3.0	0.47
I	26.31	39.8	47.9	12.3	5.6	3.4	0.49
	26.81	39.1	53.5	7.4	4.6	2.8	0.51
	27.31	36.4	50.6	13.0	6.1	3.5	0.47
	27.81	44.0	44.7	11.3	5.1	5.1	0.49
	28.33	50.1	37.2	12.7	5.0	3.0	0.35
	29.28	28.1	47.3	24.5	7.3	2.9	0.49
	29.96	40.5	47.8	11.7	5.2	1.9	0.49
	30.23	39.6	50.2	10.2	5.8	2.0	0.54
	30.66	51.4	40.5	8.2	4.3	2.0	0.48
	30.74	49.8	37.0	13.2	5.0	2.3	0.51
	30.79	40.5	37.6	21.9	9.2	1.6	0.43
	31.09	43.3	36.9	19.8	6.8	3.5	0.72
	31.39	47.0	40.6	12.4	5.1	2.7	0.40
	31.52	22.3	45.9	31.8	5.2	2.3	0.60

$$\sum n - C_{15-20} = \frac{\sum (C_{15}+C_{16}+\cdots+C_{20})}{\sum (C_{15}+C_{16}+\cdots+C_{30}+C_{31})}(\%)$$

$$\sum n - C_{21-25} = \frac{\sum (C_{21}+C_{22}+\cdots+C_{25})}{\sum (C_{15}+C_{16}+\cdots+C_{30}+C_{31})}(\%)$$

$$\sum n - C_{27-31} = \frac{\sum (C_{27}+C_{28}+\cdots+C_{31})}{\sum (C_{15}+C_{16}+\cdots+C_{30}+C_{31})}(\%)$$

$$CPI_{27-31} = \left(\frac{C_{27}+C_{29}+C_{31}}{C_{26}+C_{28}+C_{30}} + \frac{C_{27}+C_{29}+C_{31}}{C_{28}+C_{30}+C_{32}}\right) \times 0.5$$

Ste/Hop = steranes/hopanes.

were the source of at least some of the OM in this interval (Table 2; Fig. 5).

Typical $\delta^{13}C$ values of terrestrial OM range from −25.8‰ to −21.8‰ (Ando et al., 2002; Hasegawa et al., 2003; Uramoto et al., 2009; 2013). Cretaceous wood fossil has a $\delta^{13}C$ values range from −19.8‰ to −26.6‰ (Ando et al., 2002; Robinson and Hesselbo, 2004), while modern C_3 plants have a $\delta^{13}C$ range from −37‰ to −20‰, with an average of −28.5‰ (Kohn, 2010). As the $\delta^{13}C$ values of lacustrine OM are generally more depleted than those of terrestrial OM during the Cretaceous (Schnyder et al., 2009), the relatively low $\delta^{13}C_{org}$ values measured in the lower K_2n^2 (−30.2‰ to −26.9‰; Fig. 2) suggest that the OM preserved in the YWC section is predominantly derived from autochthonous lacustrine OM. However, the $\delta^{13}C_{org}$ values measured in this study are more depleted than the $\delta^{13}C$ values of lacustrine OM (−24.7‰ to −21.9‰) in the Gyeongsang Basin of Korea (Hong and Lee, 2013), which are closer to those of Cretaceous terrestrial OM. This implies that, in addition to global changes, local environments play a key role in carbon recycling. Furthermore, the depleted $\delta^{13}C_{org}$ values in Stage I may also be related to seawater incursion, as supported by the detection of C_{30} steranes (Fig. 6) and by typical Cretaceous marine OM with depleted $\delta^{13}C$ values (−28.3‰ to −22.5‰) (Sinninghe Damsté et al., 2010). Alkaline seawater entering a relatively acidic lake (Xi et al., 2011) leads to an increase in dissolved CO_2 in the lake water, which can drive the depletion of ^{13}C in the photosynthetic products (Hu et al., 2015). In addition, the depleted $\delta^{13}C_{org}$ values are consistent with the low values of Pr/Ph and high TOC and HI values (Figs. 2 and 5) in Stage I. The low Pr/Ph values together with the presence of gammacerane (Fig. 5) indicate that the lake had a shallow chemocline during this interval. Previous studies showed that chemoautotrophic bacteria and methanotrophic bacteria prevailed in the bottom water of Songliao paleolake (Wang et al., 2015) with low $\delta^{13}C_{org}$ values (Luo et al., 2014) when the shallow chemocline environment prevailed. Therefore, the depleted $\delta^{13}C_{org}$ values of OM in the lower K_2n^2 are controlled by their parent material inputs and depositional environments.

In summary, the combination of $\delta^{13}C_{org}$ values and biomarkers from the YWC section indicates a mixture of OM sources, including lacustrine algae and bacteria, aquatic macrophytes, terrigenous plants, and marine algae.

5.3. Paleoenvironmental changes during deposition of Member 2 of the Nenjiang Formation

5.3.1. Redox conditions

The isoprenoids pristane (Pr) and phytane (Ph) are present in considerable abundances in all samples (Fig. 5). According to Didyk et al. (1978), Pr/Ph ratios < 1.0 indicate anoxic conditions, while Pr/Ph ratios > 1.0 reflect oxic conditions. However, the utility of the Pr/Ph ratio as a redox indicator can be affected by variability in the maturity of the OM (ten Haven et al., 1987) and by different precursors of pristane and phytane (Goossens et al., 1984; Volkman and Maxwell, 1986; Rowland, 1990). Bechtel et al. (2012) and Wang et al. (2015) argued that the pristane and phytane in Songliao Basin sediments are derived from similar sources, as they show a consistent range of $\delta^{13}C$ values. Moreover, all samples from the YWC section were found to be immature. Therefore, the relatively low Pr/Ph ratios observed in Stage I (with the exception of two samples) are likely to be a faithful recorder of anoxic depositional conditions.

Aryl isoprenoids (1-alkyl-2,3,6-trimethyl) are derived from isorenieratane in *Chlorobiaceae,* and thus are a specific biomarker for the presence of green sulfur bacteria in the photic zone in the depositional environment (Summons and Powell, 1987). These organisms are phototrophic anaerobes that require both light and H_2S for growth, implying anoxic conditions at photic zone water depths. In modern environments, they occur in water bodies that contain sulfate and are sufficiently quiescent and organic-rich to promote sulfide production close to the photic zone (Summons, 1993). β-Carotane and isorenieratane were detected in most of samples in stages I and II. Therefore, the presence of aryl isoprenoids in stages I and II (Fig. 5) indicates a shallow chemocline environment with anoxic conditions in the bottom water expanding into the euphotic zone. The ratio of aryl isoprenoids relative to phenanthrene (A-i/P) are higher in Stage I than Stage II, implying that the water column was more anoxic in Stage I, a result that

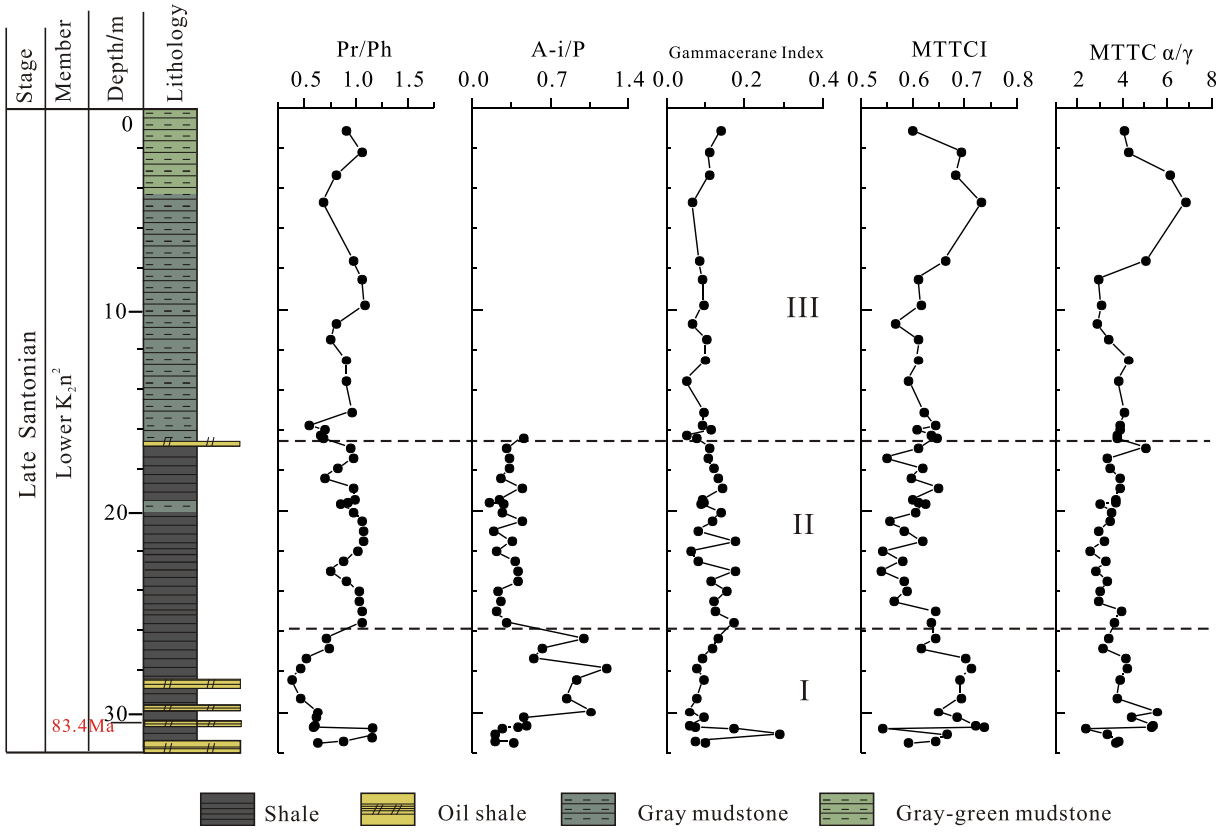

Fig. 5. Depth variation of Pr/Ph, A-i/P, the Gammacerane Index, MTTCI (α-MTTC/total MTTCs) and MTTC α/γ ratio in the YWC section.

is not consistent with variation in the Pr/Ph ratio. Aryl isoprenoids were not detected in Stage III (Fig. 5), which combined with the higher Pr/Ph ratio in this stage, suggests a relative deeper chemocline environment in this interval.

5.3.2. Water salinity

Methytrimethyltridecyl chromans (MTTCs) are similar to tocopherols, although unrelated (Peters et al., 2005). The biological source of MTTCs may be eubacteria or archaea (de Leeuw and Sinninghe Damsté, 1990); alternatively, Li et al. (1995) proposed that MTTCs derive from chlorophyll and alkylphenols during diagenesis. Regardless of their biological source, MTTCs are widely interpreted as an indicator of water column salinity (Sinninghe Damsté et al., 1993; Wang et al., 2011), with higher MTTCI values representing lower salinity (Sinninghe Damsté et al., 1987). As seen in Fig. 5, the α/γ ratio has a positive relationship with MTTCI, suggesting that both proxies reflect similar variations in paleosalinity. Variation in the MTTCI and α/γ ratio in the lower K_2n^2 suggest that the salinity of the water column was unstable. Considering variations in Pr/Ph and MTTCI, a salinity classification was proposed by Schwark et al. (1998). Wang et al. (2011) proposed an amended salinity classification with four classes: hypersaline, mesosaline, normal marine, and brackish to fresh water. Ignoring hypersaline environments, normal marine salinity is suggested when the α/γ ratio is in the range of 2–15 and the MTTCI falls between 0.4 and 0.7; mesosaline conditions are reflected by α/γ values < 2 and MTTCI values < 0.4, and fresh to brackish environments are indicated by α/γ ratios > 15 and MTTCI values > 0.7.

As shown in Fig. 7, the samples were deposited under normal marine salinity in the lower K_2n^2, which suggests a temporary marine environment for the Songliao paleolake during the lower K_2n^2. While previous studies based on the variation of the gammacerane index and MTTCI have interpreted the depositional environment as a fresh to semi-brackish lake (Wang et al., 2011; Bechtel et al., 2012), our study suggests that the differences might reflect the spatial differences of salinity in the paleolake. Wang et al. (2011) investigated samples from the SK-1 core, which is situated in the central part of the basin, whereas the outcrop investigated in our study is located in the southeast of the SLB. Moreover, the concentrations of C_{30} steranes in our study are higher than those in the previous work on SK-1 core investigated by Hu et al. (2015), which suggest that the southern part of the lake was more affected by marine incursions. This interpretation is also supported by the sediment facies, with fluvial/delta sediments deposited in the northern part of the basin (Feng et al., 2010), indicating that riverine fresh water came mostly from the north.

Gammacerane (Ga) is widely regarded as an indicator of salinity stratification in the water column during deposition (Sinninghe Damsté et al., 1995); the Gammacerane Index is calculated from the concentration of gammacerane relative to C_{30} αβ-hopane. High Gammacerane Index values are often associated with low Pr/Ph values. Therefore, the observed variation of Gammacerane Index and Pr/Ph in the lower K_2n^2 indicates variable water stratification accompanied by changes in salinity. The Gammacerane Index shows a relatively strong water stratification in Stage I, while this stratification was reduced in stages II and III.

5.4. Seawater incursion events

Specific marine biomarkers (24-*n*-propyl- and 24-iso-propylcholestanes) were identified in the YWC section indicating that marine OM was advected into the Songliao freshwater lake environment during deposition of the lower K_2n^2. The distribution of C_{30} steranes in the YWC section (Fig. 6) suggests that seawater

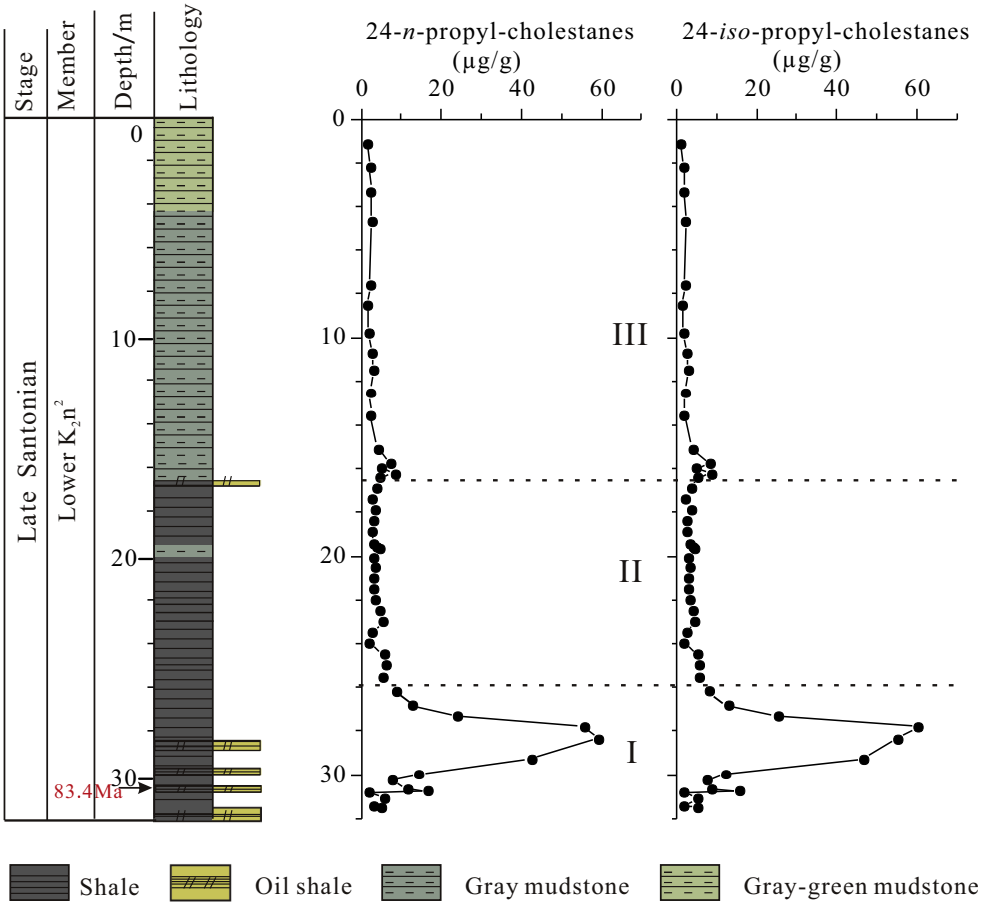

Fig. 6. Depth variation of 24-*n*-propylcholestanes and 24-isopropylcholestanes in the YWC section.

incursions were frequent in the lower K_2n^2. Concentrations of C_{30} steranes are higher in Stage I than stages II and III, indicating that greatest degree of seawater incursion occurred in the lowermost K_2n^2.

Furthermore, the YWC section shows higher concentrations of C_{30} steranes than Sk-1 core samples (Hu et al., 2015), which is likely due to the position of the YWC section closer to the marine margin. Marine planktonic foraminifera have been reliably identified from Songliao Basin strata (Xi et al., 2012, 2016), and other geochemical proxies such as C_{30} sterane biomarkers (Hu et al., 2015) and sulfur isotopes (Huang et al., 2013; Cao et al., 2016b) confirmed a marine influence on the Songliao paleolake during the Late Cretaceous. These seawater incursion events are likely controlled by tectonic activity, eustatic sea level changes, and a variable lake level (Hu et al., 2015; Xi et al., 2016).

In the early phases of K_2n^2 deposition, semi-deep to deep lacustrine facies covered the entire area of the Songliao Basin (Feng et al., 2010). Substantial rises in the lake level occurred during deposition of the lower K_2n^2 and enlarged the area covered by the lake. During the late Santonian, sea level was approximately 25–75 m higher than today (Haq, 2014). As the coast was not far from the eastern margin of the Songliao Basin (Gao et al., 1992; Hu et al., 2015), seawater ingression into the Songliao paleolake could have easily occurred when the levels of both the lake and the ocean were high. A schematic diagram of the varying paleoenvironments during deposition of lower Member 2 of the Nenjiang Formation is suggested in Fig. 8.

The Pr/Ph ratio has a negative relationship with 24-*n*-propyl- and 24-isopropyl cholestane concentrations (Fig. 9c and d), suggesting that seawater incursion events were closely related to

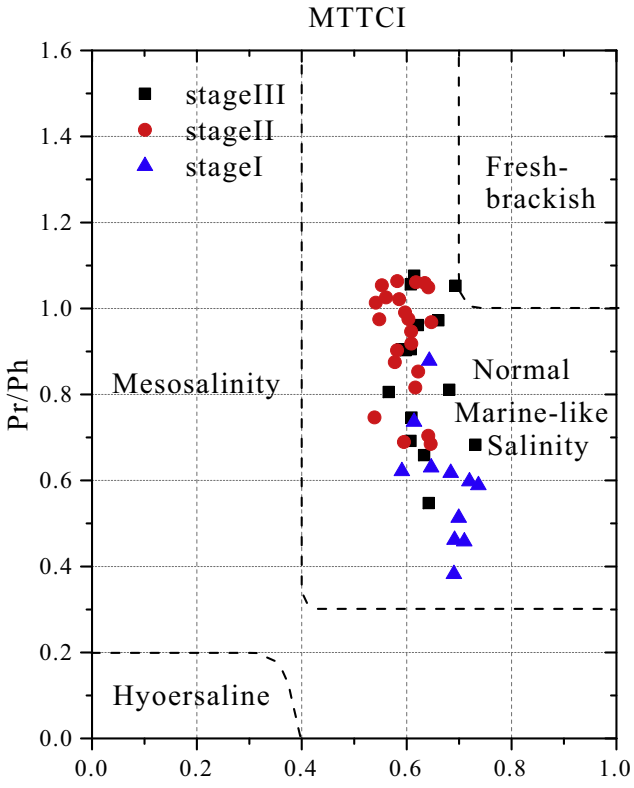

Fig. 7. Plot of Pr/Ph and MTTCI of sediments from the K_2n^2.

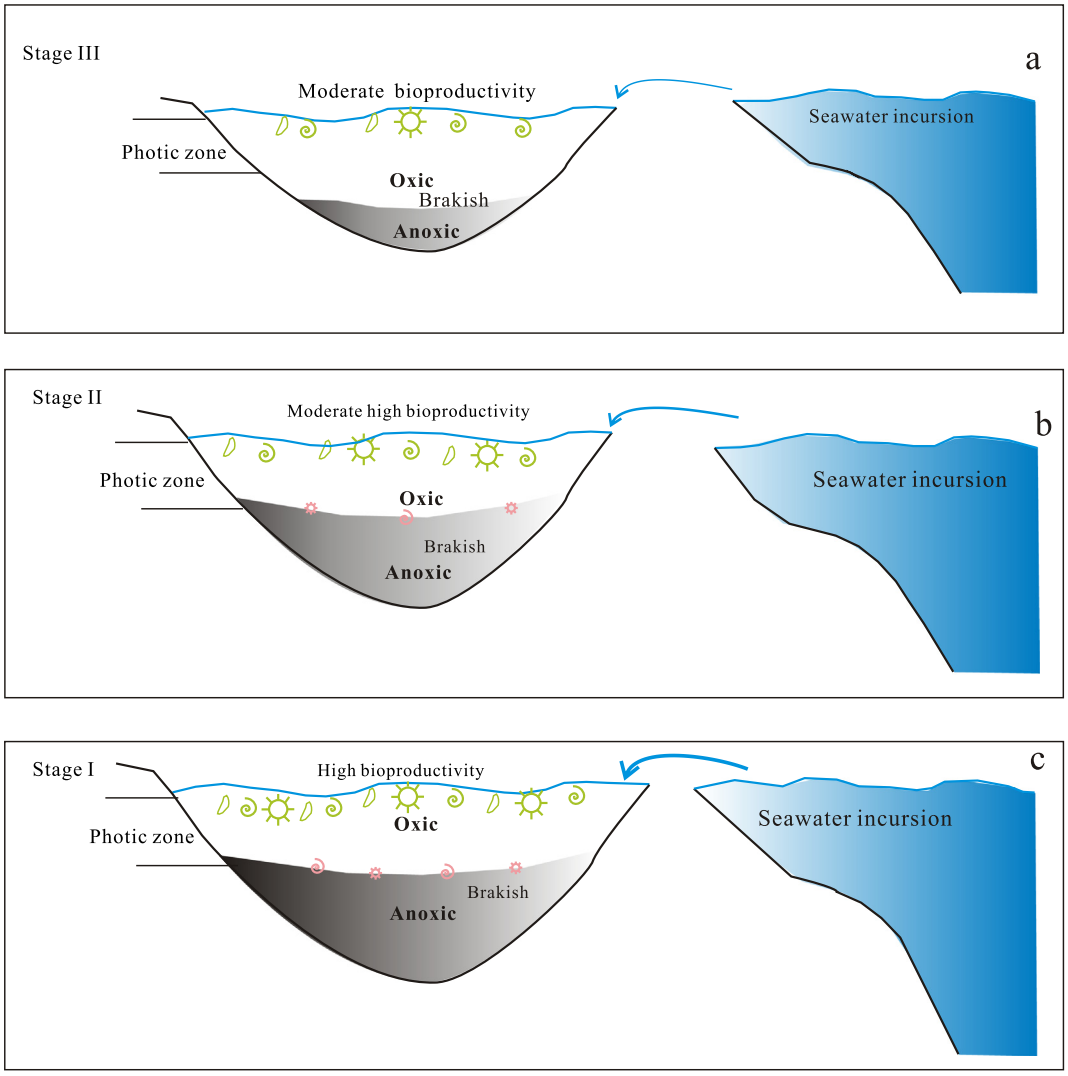

Fig. 8. Cartoon illustrating three stages of the evolution of the Songliao Basin during the lower K_2n^2 (without scale).

changes in water column redox conditions. When seawater enters a lake environment, it carries with it a load of nutrients that may promote primary productivity, driving anoxia in the bottom water. Seawater flooding into the lacustrine Songliao Basin would also be expected to increase the water salinity. Nevertheless, the MTTCI and Gammacerane Index have no obvious relationship with the concentrations of 24-*n*-propyl- and 24-isopropyl-cholestanes (Fig. 9e–h).

The area of the Songliao paleo-lake was as great as 260 000 km^2 during the K_2n^2 interval, much more extensive than during any other period of the Cretaceous (Feng et al., 2009). Therefore, this may infer that a massive influx of freshwater must have occurred, both expanding the lake's extent and diluting its salinity. Depleted δ^2H values of *n*-alkanes (Cao et al., 2016a) further support this hypothesis. The drought taxa percentages from the palynological record also indicate a relatively humid climate at 84.0 Ma in the SLB (Ji et al., 2015). In addition, the concentrations of 24-*n*-propyl- and 24-isopropyl-cholestanes show a positive relationship with TOC (Fig. 9a and b), implying that seawater incursions may have been related to the formation of organic-rich source rocks.

Another possible explanation for the high TOC intervals is that marine algae entered the paleo-lake environment every time a marine transgression occurred. However, Hu et al. (2015) argued that marine algal input was likely not the sole explanation for the high TOC in the source rocks. Another possibility is that lacustrine primary productivity increased during lower K_2n^2 deposition (Feng et al., 2009; Xi et al., 2012; Jia et al., 2013; Zhao et al., 2014), which may be partially related to enhanced nutrient availability during marine seawater incursions. In conclusion, both the high biological productivity and efficient preservation were major factors controlling OM enrichment in the lower K_2n^2.

6. Conclusions

Rock-Eval pyrolysis data indicate that the OM in Nenjiang Formation source rocks is mainly Type II and immature. The distribution of biomarker (*n*-alkanes, regular steranes, C_{30} steranes, hopanes, aryl isoprenoids) and the $\delta^{13}C_{org}$ values indicate an algal and microbial origin, with a contribution from terrigenous OM.

The lower Member 2 of the Nenjiang Formation was deposited in a stratified water column, with an intermittently anoxic photic zone during stages I and II, as indicated by the Gammacerane Index, low Pr/Ph ratios, and the presence of aryl isoprenoids. The MTTCI suggests that the sediments were deposited in a brackish environment. The presence of 24-*n*-propyl-cholestanes and 24-iso-propyl-cholestanes in the lower K_2n^2 suggests frequent but intermittent seawater incursions. High concentrations of C_{30}

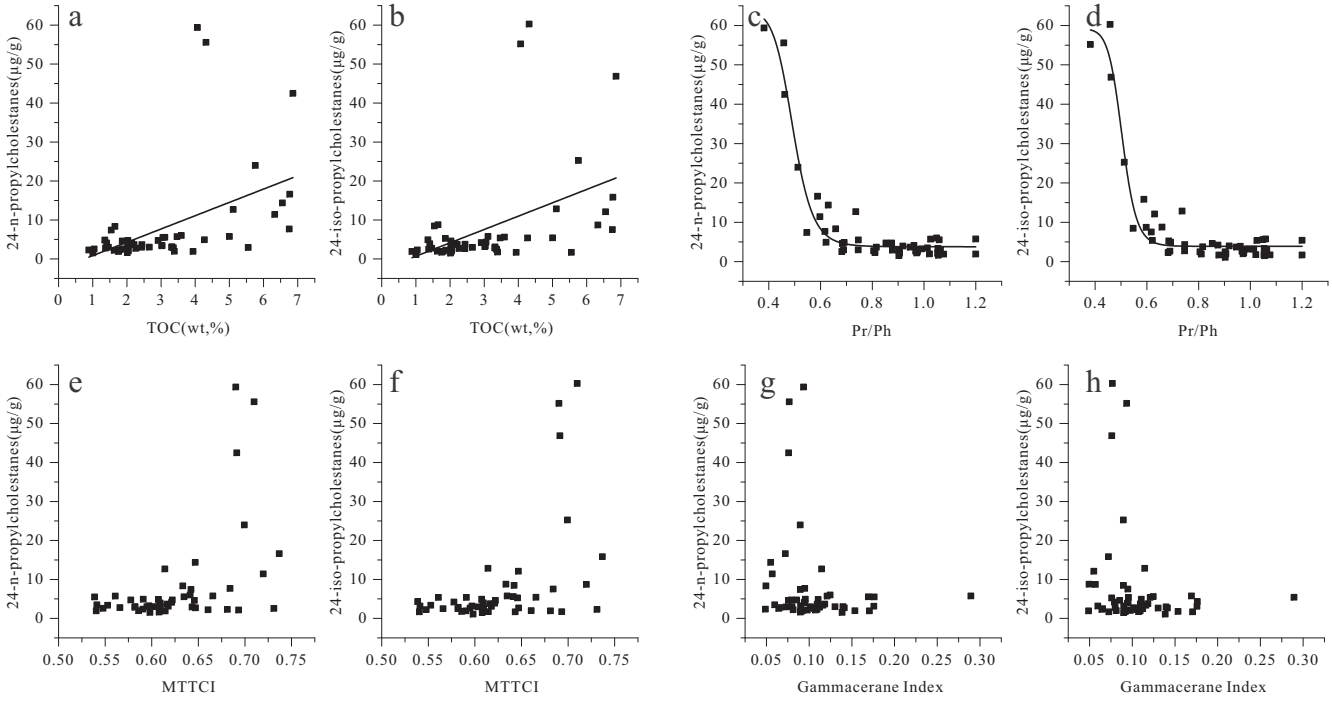

Fig. 9. Cross-correlation of: (a, b) 24-*n*-propylcholestanes/24-isopropylcholestanes vs TOC; (c, d) 24-*n*-propylcholestanes/24-isopropylcholestanes vs Pr/Ph; (e, f) 24-*n*-propylcholestanes/24-isopropylcholestanes vs MTTCI; (g, h) 24-*n*-propylcholestanes/24-isopropylcholestanes vs Gammacerane Index.

steranes are generally correlated with low Pr/Ph ratios and high A-i/P values in Stage I, implying that the seawater incursion led to aerobic and brackish conditions in the lacustrine environment. High primary productivity, combined with efficient preservation, led to substantial OM accumulation in the lower K_2n^2.

Acknowledgments

We thank Mr Zhuohuan Qin, Miss Zhongye Shi and Mr Zhiqiang Yu from China University of Geosciences (Beijing) for their help of sampling and the constructive reviews and thoughtful comments of Co-Editor in Chief John Volkman, Associate Editor Lorenz Schwark and the two anonymous reviewers are greatly appreciated. Grateful acknowledgement is given to the Western Geoscience Editing Service, which improved the quality of this manuscript. This research was financially supported by the Natural Science Foundation of China (Nos. 41790452, 41321016, 41372110) and this is also Contribution No. IS-2565 from GIGCAS.

Associate Editor—**Lorenz Schwark**

References

Ando, A., Kakegawa, T., Takashima, R., Saito, T., 2002. New perspective on Aptian carbon isotope stratigraphy: data from $\delta^{13}C$ records of terrestrial organic matter. Geology 30, 227–230.

Bechtel, A., Jia, J.L., Strobl, S.A.I., Sachsenhofer, R.F., Liu, Z.J., Gratzer, R., Püttmann, W., 2012. Palaeoenvironmental conditions during deposition of the Upper Cretaceous oil shale sequences in the Songliao Basin (NE China): implications from geochemical analysis. Organic Geochemistry 46, 76–95.

Bice, K.L., Birgel, D., Meyers, P.A., Dahl, K.A., Hinrichs, K.U., Norris, R.D., 2006. A multiple proxy and model study of Cretaceous upper ocean temperatures and atmospheric CO_2 concentrations. Paleoceanography 21, 1–17.

Bray, E.E., Evans, E.D., 1961. Distribution of *n*-paraffins as a clue to recognition of source beds. Geochimica et Cosmochimica Acta 22, 2–15.

Cao, H.R., Hu, J.F., Peng, P.A., Xi, D.P., Tang, Y.J., Lei, Y., Shilling, A., 2016a. Paleoenvironmental reconstruction of the Late Santonian Songliao Paleo-lake. Palaeogeography, Palaeoclimatology, Palaeoecology 457, 290–303.

Cao, H.S., Kaufman, A.J., Shan, X.L., Cui, H., Zhang, G.J., 2016b. Sulfur isotope constraints on marine transgression in the lacustrine Upper Cretaceous Songliao Basin, northeastern China. Palaeogeography, Palaeoclimatology, Palaeoecology 451, 152–163.

Chamberlain, C.P., Wan, X.Q., Graham, S.A., Carroll, A.R., Doebbert, A.C., Sageman, B. B., Blisniuk, P., Kent-Corson, M.L., Zhou, W., Wang, C.S., 2013. Stable isotopic evidence for climate and basin evolution of the Late Cretaceous Songliao basin, China. Palaeogeography, Palaeoclimatology, Palaeoecology 385, 106–124.

Cranwell, P.A., 1977. Organic geochemistry of Cam Loch (Sutherland) sediments. Chemical Geology 20, 205–221.

de Leeuw, J.W., Sinninghe Damsté, J.S., 1990. Organic sulfur compounds and other biomarkers as indicators of palaeosalinity. In: Wilson, L.O., White, C.M. (Eds.), Geochemistry of Sulfur in Fossil Fuels. American Chemical Society, Chichester, pp. 417–443.

Deng, C.L., He, H.Y., Pan, Y.X., Zhu, R.X., 2013. Chronology of the terrestrial Upper Cretaceous in the Songliao Basin, northeast Asia. Palaeogeography, Palaeoclimatology, Palaeoecology 385, 44–54.

Didyk, B.M., Simoneit, B.R.T., Brassell, S.C., Eglinton, G., 1978. Organic geochemical indicators of palaeoenvironmental conditions of sedimentation. Nature 272, 216–222.

Eglinton, G., Hamilton, R.J., 1967. Leaf epicuticular waxes. Science 156, 1322–1335.

Espitalié, J., Laporte, J.L., Madec, M., Marquis, F., Leplat, P., Paulet, J., Boutefeu, A., 1977. Méthode rapide de caractérisation des roches mètres, de leur potentiel pétrolier et de leur degré d'évolution. Oil Gas Science and Technology – Reviews IFP 32, 23–42.

Feng, Z.Q., Jia, C.Z., Xie, X.N., Zhang, S., Feng, Z.H., Cross, T.A., 2010. Tectonostratigraphic units and stratigraphic sequences of the nonmarine Songliao basin, northeast China. Basin Research 22, 79–95.

Feng, Z.H., Fang, W., Wang, X., Huang, C.Y., Huo, Q.L., Zhang, J.H., Huang, Q.H., Zhang, L., 2009. Microfossils and molecular records in oil shales of the Songliao Basin and implications for paleo-depositional environment. Science in China Series D: Earth Sciences 52, 1559–1571.

Ficken, K.J., Li, B., Swain, D.L., Eglinton, G., 2000. An *n*-alkane proxy for the sedimentary input of submerged/floating freshwater aquatic macrophytes. Organic Geochemistry 31, 745–749.

Friedrich, O., Norris, R.D., Erbacher, J., 2012. Evolution of middle to Late Cretaceous oceans—A 55 m.y. record of Earth's temperature and carbon cycle. Geology 40, 107–110.

Gao, R.Q., He, C.Q., Qiao, X.Y., 1992. A new genus and species of cretaceous dinoflagellates from two transgressive beds in the Songliao Basin, northeast China. Acta Palaeontologica Sinica 31, 19–30 (in Chinese with English abstract).

Gao, R.Q., Zhao, C.B., Qiao, X.Y., Zheng, Y.L., Yan, F.Y., Wan, C.B., 1999. Cretaceous Oil Strata Palynology from Songliao Basin. Geological Publishing House, Beijing, pp. 25–373 (in Chinese).

Goossens, H., de Leeuw, J.W., Schenck, P.A., Brassell, S.C., 1984. Tocopherols as likely precursors of pristane in ancient sediments and crude oils. Nature 312, 440–442.

Haq, B.U., 2014. Cretaceous eustasy revisited. Global and Planetary Change 113, 44–58.

Haq, B.U., Hardenbol, J., Vail, P.R., 1987. Chronology of fluctuating sea levels since the Triassic. Science 235, 1156–1167.
Hasegawa, T., Pratt, L., Maeda, H., Shigeta, Y., Okamoto, T., Kase, T., Uemura, K., 2003. Upper Cretaceous stable carbon-isotope stratigraphy of terrestrial organic matter from Sakhalin, Russian Far East: a proxy for the isotopic composition of paleoatmospheric CO_2. Palaeogeography, Palaeoclimatology, Palaeoecology 215, 179–182.
He, H.Y., Deng, C.L., Wang, P.J., Pan, Y.X., Zhu, R.X., 2012. Toward age determination of the termination of the Cretaceous Normal Superchron. Geochemistry, Geophysics, Geosystems 13, 1–20.
Hong, S.K., Lee, Y.I., 2013. Contributions of soot to $\delta^{13}C$ of organic matter in Cretaceous lacustrine deposits, Gyeongsang Basin, Korea: implication for paleoenvironmental reconstructions. Palaeogeography, Palaeoclimatology, Palaeoecology 371, 54–61.
Hou, D., Li, M., Huang, Q., 2000. Marine transgressional events in the gigantic freshwater Lake Songliao: paleontological and geochemical evidence. Organic Geochemistry 31, 763–768.
Hu, J.F., Peng, P.A., Liu, M.Y., Xi, D.P., Song, J.Z., Wan, X.Q., Wang, C.S., 2015. Seawater incursion events in a Cretaceous paleo-lake revealed by specific marine biological markers. Scientific Reports 5, 9508. https://doi.org/10.1038/srep09508.
Hu, X.M., Wagreich, M., Yilmaz, I.O., 2012. Marine rapid environmental/climatic change in the Cretaceous greenhouse world. Cretaceous Research 38, 1–6.
Huang, Y.J., Yang, G.S., Gu, J., Wang, P.K., Huang, Q.H., Feng, Z.H., Feng, L.J., 2013. Marine incursion events in the Late Cretaceous Songliao Basin: constraints from sulfur geochemistry records. Palaeogeography Palaeoclimatology Palaeoecology 385, 152–161.
Jenkyns, H.C., 2010. Geochemistry of oceanic anoxic events. Geochemistry, Geophysics, Geosystems 11, 427–428.
Ji, L.M., Zhang, M.Z., Song, Z.G., 2015. The palynological record from Coniacian to lower Campanian continental sequences in the Songliao Basin, northeastern China and its implications for palaeoclimate. Cretaceous Research 56, 226–236.
Jia, J.L., Bechtel, A., Liu, Z.J., Strobl, S.A.I., Sun, P.C., Sachsenhofer, R.F., 2013. Oil shale formation in the Upper Cretaceous Nenjiang Formation of the Songliao Basin (NE China): implications from organic and inorganic geochemical analyses. International Journal of Coal Geology 113, 11–26.
Kodner, R.B., Pearson, A., Summons, R.E., Knoll, A.H., 2008. Sterols in red and green algae: quantification, phylogeny, and relevance for the interpretation of geologic steranes. Geobiology 6, 411–420.
Kohn, M.J., 2010. Carbon isotope compositions of terrestrial C3 plants as indicators of (paleo)ecology and (paleo)climate. Proceedings of the National Academy of Sciences of the United States of America 107, 19691–19695.
Lafargue, E., Marquis, F., Pillot, D., 1998. Rock-Eval 6 applications in hydrocarbon exploration, production, and soil contamination studies. Oil Gas Science and Technology – Reviews IFP 53, 421–437.
Li, M.W., Larter, S.R., Taylor, P., Jones, D.M., Bowler, B., Bjorøy, M., 1995. Biomarkers or not biomarkers? A new hypothesis for the origin of pristane involving derivation from methyltrimethyltridecylchromans (MTTCs) formed during diagenesis from chlorophyll and alkylphenols. Organic Geochemistry 23, 159–167.
Love, G.D., Grosjean, E., Stalvies, C., Fike, D.A., Grotzinger, J.P., Bradley, A.S., Kelly, A. E., Bhatia, M., Meredith, W., Snape, C.E., 2009. Fossil steroids record the appeaarance of demospongiae during the Cryogenian period. Nature 457, 718–722.
Luo, G., Junium, C.K., Kump, L.R., Huang, J., Li, C., Feng, Q., Shi, X., Bai, X., Xie, S., 2014. Shallow stratification prevailed for 1700 to 1300 Ma ocean: evidence from organic carbon isotopes in the North China Craton. Earth and Planetary Science Letters 400, 219–232.
Mackenzie, A.S., Beaumont, C., McKenzie, D.P., 1984. Estimation of the kinetics of geochemical reactions with geophysical models of sedimentary basins and applications. Organic Geochemistry 6, 875–884.
Metzger, P., Largeau, C., Casadevall, E., 1991. Lipids and macromolecular lipids of the hydrocarbon-rich microalga *Botryococcus braunii*. Chemical structure and biosynthesis. Geochemical and biotechnological importance. In: Herz, W., Kirby, G.W., Steglich, W., Tamm, C. (Eds.), Progress in the Chemistry of Organic Natural Products. Springer Verlag, Berlin, pp. 1–70.
Moldowan, J.M., 1984. C_{30}-steranes, novel markers for marine petroleums and sedimentary rocks. Geochimica et Cosmochimica Acta 48, 2767–2768.
Moldowan, J.M., Fago, F.J., Lee, C.Y., Jacobson, S.R., Watt, D.S., Slougui, N.E., Jeganathan, A., Young, D.C., 1990. Sedimentary 24-*n*-propylcholestanes, molecular fossils diagnostic of marine algae. Science 247, 309–312.
Peters, K.E., Walters, C.C., Moldowan, J.M., 2005. The Biomarker Guide. Biomarkers and Isotopes in Petroleum Exploration and Earth History. Cambridge University Press, New York.
Robinson, S.A., Hesselbo, S.P., 2004. Fossil-wood carbon-isotope stratigraphy of the non-marine Wealden Group (Lower Cretaceous, southern England). Journal of the Geological Society 161, 133–145.
Rowland, S.J., 1990. Production of acyclic isoprenoid hydrocarbons by laboratory maturation of methanogenic bacteria. Organic Geochemistry 15, 9–16.
Schlanger, S.O., Jenkyns, H.C., 1976. Cretaceous oceanic anoxic events: cause and consequence. Geologie en Mijnbouw 55, 179–184.
Schnyder, J., Dejax J., Keppens, E., Nguyen Tu, T.T., Spagna, P., Boulila, S., Galbrun, B., Riboulleau, A., Tshibangu, J-P., Yans, J., 2009. An Early Cretaceous lacustrine record: organic matter and organic carbon isotopes at Bernissart (Mons Basin, Belgium). Palaeogeography, Palaeoclimatology, Palaeoecology **281**, 79–91.
Schwark, L., Vliex, M., Schaeffer, P., 1998. Geochemical characterization of Malm Zeta laminated carbonates from the Franconian Alb, SW-Germany (II). Organic Geochemistry 29, 1921–1952.
Sinninghe Damsté, J.S., Koek-van Dalen, A.C., de Leeuw, J.W., Schenck, P.A., Sheng, G. Y., Brassell, S.C., 1987. The identification of mono-, di- and trimethyl 2-(4,8,12-trimenthyltridecyl) chromans and their occurrence in the geosphere. Geochimica et Cosmochimica Acta 51, 2393–2400.
Sinninghe Damsté, J.S., Rijpstra, W.I.C., de Leeuw, J.W.D., Schenck, P.A., 1989. The occurrence and identification of series of organic sulphur compounds in oils and sediment extracts: II. Their presence in samples from hypersaline and non-hypersaline palaeoenvironments and possible application as source, palaeoenvironmental and maturity indicators. Geochimica et Cosmochimica Acta 53, 1323–1341.
Sinninghe Damsté, J.S., Keely, B.J., Betts, S.E., Baas, M., Maxwell, J.R., de Leeuw, J.W., 1993. Variations in abundances and distributions of isoprenoid chromans and long-chain alkylbenzenes in sediments of the Mulhouse Basin: a molecular sedimentary record of palaeosalinity. Organic Geochemistry 20, 1201–1215.
Sinninghe Damsté, J.S., Kenig, F., Koopmans, M.P., Köster, J., Schouten, S., Hayes, J.M., de Leeuw, J.W., 1995. Evidence for gammacerane as an indicator of water column stratification. Geochimica et Cosmochimica Acta 59, 1895–1900.
Sinninghe Damsté, J.S., Koopmans, M.P., 1997. The fate of carotenoids in sediments: an overview. Pure and Applied Chemistry 69, 2067–2074.
Sinninghe Damsté, J.S., van Bentum, E.C., Reichart, G.-J., Pross, J., Schouten, S., 2010. A CO_2 decrease-driven cooling and increased latitudinal temperature gradient during the mid-Cretaceous Oceanic Anoxic Event 2. Earth and Planetary Science Letters 293, 97–103.
Skelton, P.W., Spicer, R.A., Kelley, S.P., Gilmour, I., 2003. The Cretaceous World. Cambridge University Press, London.
Summons, R.E., Powell, T.G., 1987. Identification of aryl isoprenoids in source rocks and crude oils: biological markers for the green sulphur bacteria. Geochimica et Cosmochimica Acta 51, 557–566.
Summons, R.E., Barrow, R.A., Capon, R.J., Hope, J.M., Stranger, C., 1993. The structure of a new C_{25} isoprenoid alkene biomarker from diatomaceous microbial communities. Australian Journal of Chemistry 46, 907–915.
ten Haven, H.L., de Leeuw, J.W., Rullkötter, J., Sinninghe Damsté, J.S., 1987. Restricted utility of the pristane/phytane ratio as a palaeoenvironmental indicator. Nature 330, 641–643.
Tissot, B.P., Durand, B., Espitalié, J., Combaz, A., 1974. Influence of the nature and diagenesis of organic matter in formation of petroleum. American Association of Petroleum Geologists Bulletin 58, 499–506.
Uramoto, G.I., Abe, Y., Hirano, H., 2009. Carbon isotope fluctuations of terrestrial organic matter for the Upper Cretaceous (Cenomanian–Santonian) in the Obira area, Hokkaido, Japan. Geological Magazine 146, 761–774.
Uramoto, G.I., Tahara, R., Sekiya, T., Hirano, H., 2013. Carbon isotope stratigraphy of terrestrial organic matter for the Turonian (Upper Cretaceous) in northern Japan: implications for ocean-atmosphere $\delta^{13}C$ trends during the mid-Cretaceous climatic optimum. Geosphere 9, 355–366.
Volkman, J.K., 1986. A review of sterol markers for marine and terrigenous organic matter. Organic Geochemistry 9, 83–99.
Volkman, J.K., Maxwell, J.R., 1986. Acyclic isoprenoids as biological markers. In: Johns, R.B. (Ed.), Biological Markers in the Sedimentary Record. Elsevier, Amsterdam, pp. 1–42.
Volkman, J.K., Barrett, S.M., Blackburn, S.I., Mansour, M.P., Sikes, E.L., Gelin, F., 1998. Microalgae biomarkers: a review of recent research developments. Organic Geochemistry 29, 1163–1179.
Wan, X.Q., Wu, H.C., Xi, D.P., Liu, M.Y., Qin, Z.H., 2017. Terrestrial biota and climate during Cretaceous greenhouse in NE China. Earth Science Frontiers 24, 18–31 (in Chinese with English Abstracts).
Wang, C.S., Feng, Z.Q., Zhang, L.M., Huang, Y.J., Cao, K., Wang, P.J., Zhao, B., 2013. Cretaceous paleogeography and paleoclimate and the setting of SKI borehole sites in Songliao Basin, northeast China. Palaeogeography, Palaeoclimatology, Palaeoecology 385, 17–30.
Wang, L., Song, Z.G., Yin, Q., George, S.C., 2011. Paleosalinity significance of occurrence and distribution of methyltrimethyltridecyl chromans in the Upper Cretaceous Nenjiang Formation, Songliao Basin, China. Organic Geochemistry 42, 1411–1419.
Wang, L., Song, Z.G., Cao, X.X., Li, Y., 2015. Compound specific carbon isotope study on the hydrocarbon biomarkers in lacustrine source rocks from Songliao Basin. Organic Geochemistry 87, 68–77.
Wang, P.J., Mattern, F., Didenko, N.A., Zhu, D.F., Singer, B., Sun, X.M., 2016a. Tectonics and cycle system of the Cretaceous Songliao Basin: an inverted active continental margin basin. Earth-Science Reviews 159, 82–102.
Wang, T.T., Ramezani, J., Wang, C.S., Wu, H.C., He, H.Y., Bowring, S.A., 2016b. High-precision U-Pb geochronologic constraints on the Late Cretaceous terrestrial cyclostratigraphy and geomagnetic polarity from the Songliao Basin, Northeast China. Earth and Planetary Science Letters 446, 37–44.
Wu, H.C., Zhang, S.H., Jiang, G.Q., Hinnov, L., Yang, T.S., Li, H.Y., Wan, X.Q., Wang, C.S., 2013. Astrochronology of the Early Turonian-Early Campanian terrestrial succession in the Songliao Basin, northeastern China and its implication for long-period behavior of the Solar System. Palaeogeography, Palaeoclimatology, Palaeoecology 385, 55–70.
Wu, H.C., Zhang, S.H., Hinnov, L.A., Jiang, G.Q., Yang, T.S., Li, H.Y., Wan, X.Q., Wang, C. S., 2014. Cyclostratigraphy and orbital tuning of the terrestrial upper Santonian-Lower Danian in Songliao Basin, northeastern China. Earth and Planetary Science Letters 407, 82–95.

Xi, D.P., Wan, X.Q., Jansa, L., Zhang, Y.Y., 2011. Late Cretaceous paleoenvironment and lake level fluctuation in the Songliao Basin, northeastern China. Island Arc 20, 6–22.

Xi, D.P., Li, S., Wan, X.Q., Jing, X., Huang, Q.H., Colin, J.P., Wang, Z., Si, W., 2012. Late Cretaceous biostratigraphy and paleoenvironmental reconstruction based on non-marine ostracodes from well SK1 (south), Songliao Basin, northeast China. Hydrobiologia 688, 113–123.

Xi, D.P., Cao, W.X., Huang, Q.H., Do Carmo, D.A., Li, S., Jing, X., Tu, Y.J., Jia, J.Z., Qu, H. Y., Zhao, J., Wan, X.Q., 2016. Late Cretaceous marine fossils and seawater incursion events in the Songliao Basin, NE China. Cretaceous Research 62, 172–182.

Xie, L.H., Spiro, B., Wei, G.J., 2016. Purification of $BaSO_4$ precipitate contaminated with organic matter for oxygen isotope measurements ($\delta^{18}O$ and $\Delta^{17}O$). Rapid Communications in Mass Spectrometry 30, 1727–1733.

Yu, Z.Q., 2017. Zircon U-Pb chronology of Cretaceous Yingcheng Formation and Nenjiang Formation in the Songliao Basin (in Chinese with English abstract) China University of Geosciences (Beijing).

Zhao, J., Wan, X., Xi, D., Jing, X., Li, W., Huang, Q., Zhang, J., 2014. Late Cretaceous palynology and paleoclimate change: evidence from the SK1 (South) core, Songliao Basin, NE China. Science China Earth Sciences 57, 2985–2997.